Decadal Oscillations in a Simple Coupled Model

MATTHIAS MÜNNICH, MOJIB LATIF, STEPHAN VENZKE, AND ERNST MAIER-REIMER

Max-Planck-Institut für Meteorologie, Hamburg, Germany

(Manuscript received 24 October 1997, in final form 13 January 1998)

ABSTRACT

To study the dynamics that may lead to decadal oscillations in the North Pacific a simple coupled model is developed. The ocean is based on the linear, potential vorticity equation for baroclinic planetary waves. The atmosphere is reduced to a nonlocal wind response to thermocline depth anomalies. The wind stress has a spatially fixed structure and its amplitude depends on the thermocline perturbation at one location or in a predefined index region.

Such a simple coupled model produces decadal oscillations for suitable parameter choices. For realistic wind stress patterns, the patterns of oceanic variability are similar to those observed. It is determined by the speed of long Rossby waves at the coupling latitude. The period of the oscillation is rather insensitive to the coupling strength and amounts to approximately twice the time the Rossby wave needs to travel from the center of the wind stress curl anomaly to the coupling location.

A stochastic component to the atmospheric forcing is incorporated by white noise added to the feedback. With such a forcing, typical oceanic spectra become red with a broad peak at decadal timescales superimposed.

1. Introduction

Large-scale climate variations in the North Pacific climate system on decadal timescale are well documented (Douglas et al. 1982; Trenberth 1990; Wallace et al. 1993; Deser et al. 1996; Zhang and Levitus 1997). Various hypotheses have been put forward to explain these decadal fluctuations. The ''stochastic climate scenario'' of Hasselmann (1976), favored in a number of studies (e.g., Frankignoul et al. 1997), states that the observed variations are simply the long-frequency tail of a purely red spectrum that arises from the integration of the atmospheric noise by the ocean. Indeed, the decadal signal is weak and the observational record is relatively short, which makes it difficult to identify spectral peaks at decadal time scales.

Other, more dynamical explanations have been proposed. Trenberth and Hurrel (1994) and Graham (1994) emphasize the role of the Tropics as the major driving force for the decadal variability in the North Pacific. Graham (1994) sees evidence that the last phase shift from a warm to a cold North Pacific was caused by a change in tropical Pacific SST that introduced a change in the strength of the Aleutian low via established teleconnections. Furthermore, Trenberth and Hurrel (1994) also emphasize the role of the positive feedback mechanisms between the ocean and the atmosphere in the North Pacific itself. These feedback mechanisms were originally hypothesized by Namias (1959, 1969) and Bjerknes (1964): an anomalously warm North Pacific reduces the north–south surface temperature difference and thus deminishes the driving agent for the North Pacific storm track. The weakened winds strengthen the SST anomaly by a number of processes (reduced heat loss to the atmosphere, reduced oceanic mixing, and enhanced poleward transport of heat by anomalous Ekman currents). Simultaneously the wind-driven subtropical gyre weakens in response to the associated change in wind stress curl. Thus, less heat is transported into the North Pacific, which reduces the SST tendency, and the inertia of the gyre leads to a phase reversal into a colder than normal North Pacific. Latif and Barnett (1994, 1996, hereafter LB94 and LB96) analyzed the decadal climate variability in the ''ECHO'' coupled ocean–atmosphere general circulation model (GCM) and judge these feedback mechanisms as the primary agents for the decadal variability. They found that the sensitivity of the atmosphere to North Pacific temperature variation is much larger than expected and concluded that tropical interactions may be unnecessary for the existence of the North Pacific decadal climate mode.

In this study we further investigate the feedbacks that lead to the decadal variability in the North Pacific. We focus on the dynamics in the ocean while the atmo-

Corresponding author address: Dr. Matthias Münnich, Max-Planck-Institut für Meteorologie, Bundesstraße 55, 20146 Hamburg, Germany.
E-mail: muennich@dkrz.de

spheric dynamics and the thermodynamics in the ocean are only crudely parameterized. We neglect the internal atmospheric dynamics, which is based on the assumption that the atmosphere is in a statistical equilibrium with the sea surface temperature (SST) on decadal timescales.

This article is organized as follows. In section 2 we review aspects of the Rossby wave dynamics relevant to this problem and introduce the numerical model we use in our study. Section 3 describes the atmospheric feedback and discusses the dependence of the model on various parameters. The model is tuned to observations in section 4. The stochastic component of the atmospheric forcing is included in section 5. In the final section 6 we discuss our results, draw some conclusions, and give an outlook for possible future work.

2. The model

The large-scale circulation of the oceans in midlatitudes is known to be governed by the potential vorticity equation (e.g., Rhines 1986). As the adjustment time for the barotropic mode is of the order of weeks, while the baroclinic adjustment timescale is several years, only the baroclinic response should be dynamically important for the decadal variability problem. Therefore, and to keep matters simple, we use a reduced gravity model for the first baroclinic mode. The model dynamics are kept linear, so only small fluctuations around the mean state of the ocean are well represented. The governing equation is the linear potential vorticity equation, which reads on the beta plane at latitude θ_0;

$$\left[p_{xx} + p_{yy} - \frac{f^2}{c^2}p\right]_t + \beta p_x = F,$$

$$F = \frac{f}{H}(\tau^y_x - \tau^x_y). \qquad (1)$$

Here p denotes the pressure anomaly of the baroclinic mode divided by density, x and y are the zonal and meridional directions at latitude θ_0, c is the gravity wave speed of the baroclinic mode considered, f denotes the Coriolis parameter, β its meridional derivative, and subscripts denote partial derivatives. Here, H is a measure of how well the wind stress projects onto the mode the so-called forcing depth (Gill 1982). The zonal and meridional wind stress anomalies are denoted by τ^x and τ^y. The free wave solutions of this equation ($F \equiv 0$) are the planetary Rossby waves. Assuming a plane wave, $p = p_0 \exp[i(kx + ly - \omega t)]$, the dispersion relation and group velocity c_g are easily derived from (1). For the latter, one obtains

$$c_g = \beta\frac{k^2 - l^2 - R^{-2}}{(k^2 + l^2 + R^{-2})^2}, \qquad (2)$$

with $R = c/f$ being the Rossby radius. The group velocity reaches its maximum speed βR^2 for the largest scale modes, that is, if both k and l vanish. For these basin-size waves the group velocities are negative, and the waves are moving to the west. Equation (1) allows eastward traveling waves as well. Their group velocity is about an order of magnitude slower. The wavelengths of these waves are of the order of the Rossby deformation radius of about 30 km. These short Rossby waves are important to the formation of the western boundary currents. We assume here that these waves are too short to be relevant to the large-scale decadal variations we like to model. Neelin and Weng (1998) and Weng and Neelin (1998, manuscript submitted to *J. Climate*) include these waves in their analytical model and obtain similar result as we do, which justifies the neglect of the short Rossby waves.

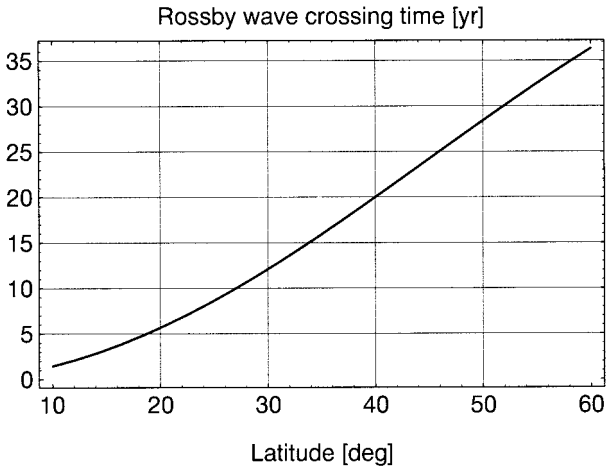

FIG. 1. Dependence of the traveling time of the longest Rossby wave across the Pacific on latitude. The Pacific basin is approximated by a sector of 100° longitude. The baroclinic gravity wave speed is set to 2.6 m s^{-1}.

For constant forcing Anderson and Gill (1975, hereafter AG75) note two solutions of the forced problem (1): the space-independent solution

$$p(t) = -R^2Ft, \qquad (3)$$

and the time-independent Sverdrup solution

$$p(x) = F\beta^{-1}x. \qquad (4)$$

AG75 shows how the solution of (1) transforms from the first to the second solution during spinup. The dependence of the group velocity of the long Rossby waves on β makes their velocity strongly dependent on the latitude θ_0. The typical Rossby wave crossing times in the North Pacific are illustrated in Fig. 1. The transit time quadruples from about 5 yr in the Tropics near 20°N to about 20 yr in midlatitudes near 40°N. Our area of interest spans an even wider latitude band, so that a β-plane approximation is not appropriate. The equation that corresponds to (1) on the sphere reads (AG75)

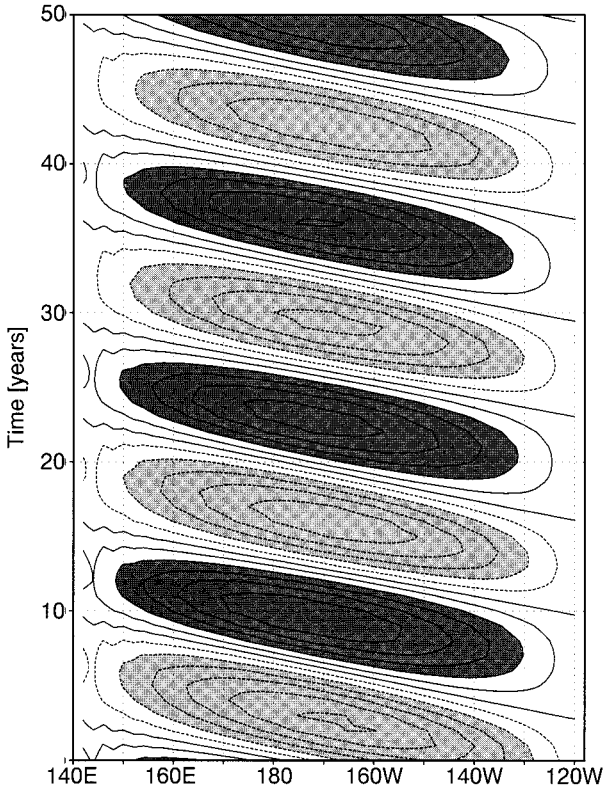

FIG. 2. Hovmöller diagram of the pressure anomalies at the coupling latitude 30°N. The coupling point is located close to the western boundary at 30°N, 142°E.

$$\left[\left(\frac{\cos\theta}{a^2\sin^2\theta}p_\theta\right)_\theta + \frac{1}{a^2\cos\theta\sin^2\theta}p_{\phi\phi} - \cos\theta\left(\frac{2\Omega}{c}\right)^2 p\right]_t + \frac{2\Omega\cos\theta}{a^2\sin^2\theta}p_\phi = \tilde{F}, \tag{5}$$

with

$$\tilde{F} = \frac{2\Omega}{aH}\left[\frac{\tau^y_\phi}{\sin\theta} - \left(\frac{\tau^x\cos\theta}{\sin\theta}\right)_\theta\right], \tag{6}$$

or using the longitudinal and meridional coordinates $x = a(\cos\theta)\phi$ and $y = a\theta$

$$\left[p_{xx} + p_{yy} + \frac{1+\cos^2(y/a)}{a\sin(y/a)\cos(y/a)}p_y - R^{-2}p\right]_t + \beta p_x = F,$$

with

$$F = \frac{f}{H}\left[\tau^y_x - \tau^x_y + \frac{\tau^x}{a\sin(y/a)\cos(y/a)}\right]. \tag{7}$$

Here a is the radius and Ω the angular frequency of the earth. Equation (7) shows that (1) with varying f and β is a good approximation of (6), as long as the meridional scale is much smaller than the radius of the earth a. However, we do not use this simplification because (6) is no harder to solve numerically than (1). Our model solves (6) on a $2° \times 2°$ grid by an implicit finite-differencing scheme. The model domain is a flat, rectangular longitude–latitude box, extending from 14°–

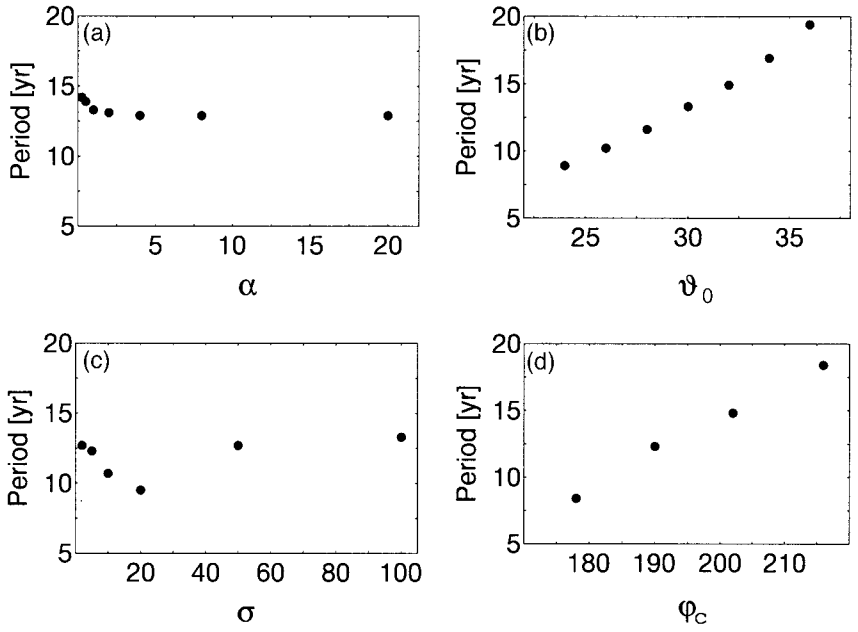

FIG. 3. Parameter dependence of the oscillation period; shown are the dependences of the period on (a) the coupling strength α, (b) latitude θ_0 of the coupling point, (c) width σ of the forcing pattern, and (d) the longitudinal location ϕ_c of the center of the wind stress curl anomaly.

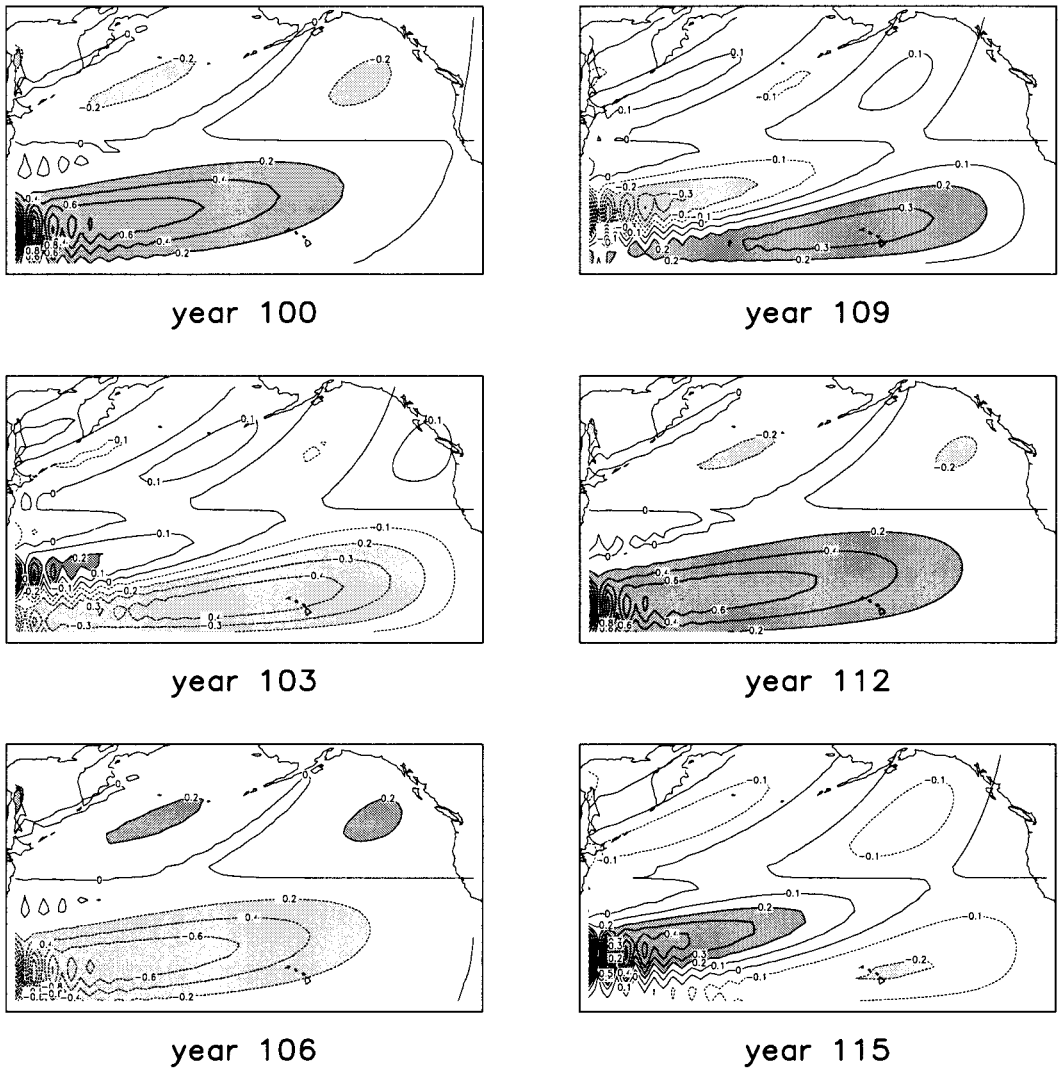

FIG. 4. Snapshots of thermocline depth anomalies for the same run as in Fig. 2.

64°N, 140°E–120°W. We use a constant baroclinic gravity wave speed of $c = 2.6$ m s^{-1}. A harmonic viscous term $\nu(p_{xx} + p_{yy})$, with $\nu = 3000$ s^{-1}, is added on the rhs of (6) for numerical reasons. As boundary conditions we use $p = \text{const}$ along the boundary. For a two-layer model with relative density difference $\delta\rho = (\rho_2 - \rho_1)/\rho_2$ the pressure anomaly p and the anomalous height of the layer interface h (i.e., the thermocline depth anomaly) are related by $p = \delta\rho g h$. Therefore, we shall often consider our model as a model for the thermocline depth anomaly and identify p with a (normalized) thermocline depth anomaly.

The forcing of the ocean by the atmospheric wind stress curl remains to be specified. LB94 found that a positive SST anomaly in the North Pacific weakens the Aleutian low and thus changes the wind stress curl in midlatitudes and the subtropics. There is no temperature equation in our model, and we assume the feedback to be directly dependent on the thermocline depth anomaly. We introduce a feedback from the ocean to the atmosphere by linking the wind stress anomaly directly to the thermocline depth. The spatial structure of the wind forcing function F will be kept constant, that is, we use

$$F(t, \theta, \phi) = A(t)X_0(\theta, \phi). \tag{8}$$

Here $X_0(\theta, \phi)$ is the wind stress curl pattern. The feedback from the ocean to the atmosphere will be introduced by letting the amplitude A of the wind stress forcing F depend on the current thermocline depth anomaly p of the ocean.

3. Parameter study

As a first example, we report results using an artificial sinusoidal forcing pattern

$$X_0 = X_m \sin[2\pi(\theta - \theta_c)/B],$$

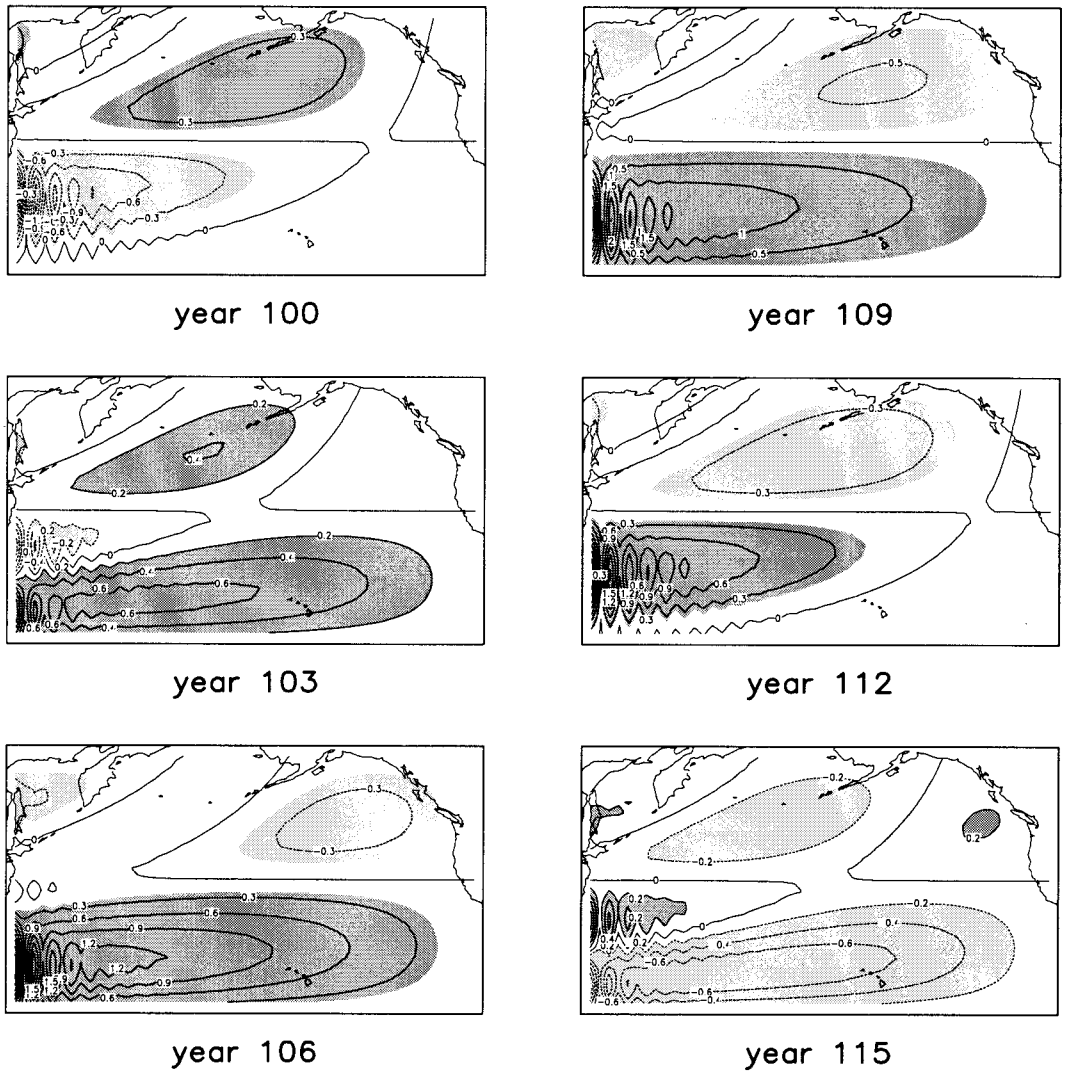

FIG. 5. Same as Fig. 4 for a coupling at 42°N, 142°E.

with $\theta_c = 30°$N and the meridional extent of the basin, $B = 26°$. The way in which the wind stress amplitude A depends on the thermocline depth anomaly remains to be specified. To study the behavior of the system we relate the amplitude A linearly to the thermocline depth anomaly $p(\theta_0, \phi_0)$ at a fixed point (θ_0, ϕ_0)[1]: $A(t) = \alpha p(\theta_0, \phi_0, t)$ with $\theta_0 = 40°$N. We choose $X_m = 3 \times 10^{-14}$ s^{-3} and use a forcing depth $H = 1500$ m that corresponds for $A = 1$ to a wind stress curl anomaly of 4.5×10^{-7} Pa m^{-1}. The model is initialized by a broad thermocline depth anomaly in the central North Pacific. Figure 2 shows a Hovmöller diagram of the thermocline depth anomaly at the coupling latitude. The coupling is located near the eastern boundary at 30°N and the coupling parameter $\alpha = 1$. The model shows a weakly damped periodic oscillation with a period of about 13 yr. The anomalies appear in the eastern part of the basin first and propagate to the west with the phase speed of the long Rossby waves.

We found that the period of the oscillation is rather insensitive to the coupling strength α. It is about twice the time the long Rossby waves need to travel from the center of the forcing to the coupling point, where they excite the feedback. As noted above (Fig. 1), the Rossby wave speed is strongly dependent on latitude, which is reflected in a pronounced sensitivity of the oscillation period on the latitude of the coupling point. Moving the coupling to the east shortens the period by reducing the distance the anomaly signal has to travel to the coupling

[1] Experiments were also performed with a feedback proportional to the north–south temperature difference in the western Pacific. This form of coupling can be motivated by the cyclogenesis in this region which is driven by the north–south temperature difference. The results are similar to the point coupling discussed here.

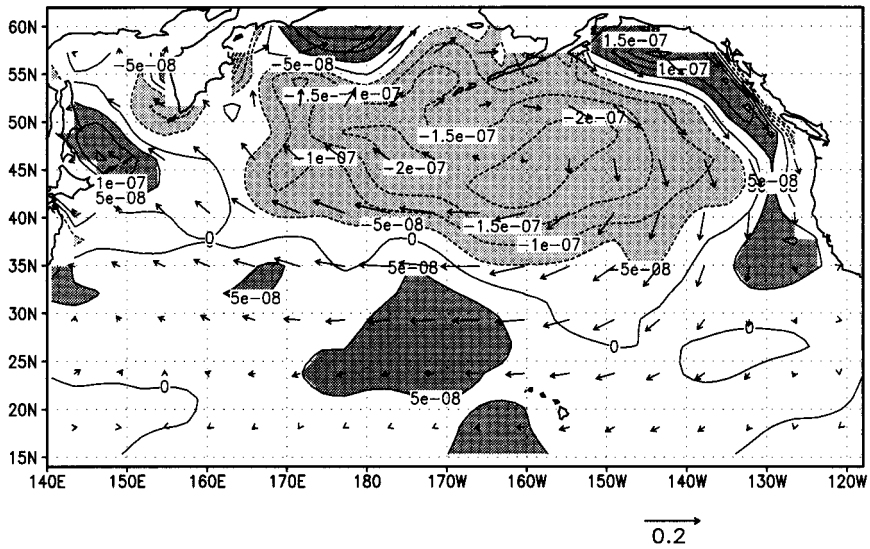

FIG. 6. Response of the atmospheric GCM ECHAM3 to a SST anomaly centered over the North Pacific. Shown is the resulting wind stress anomaly (arrows) and its curl (contours).

point. This and some other parameter dependencies of the oscillation period are illustrated in Fig. 3 for the forcing function

$$A(t) = \alpha A_0 p(\theta_0, \phi_0, t),$$

$$X_0(\theta, \phi) = \sin\left(2\pi \frac{\theta - \theta_c}{B}\right) \exp\left[-\left(\frac{\phi - \phi_c}{\sigma}\right)^2\right],$$

with the parameter values of Fig. 2 as the reference values, that is, $\alpha = 1$, $\theta_0 = 30°$, $\phi_0 = 142°$, and $\sigma = \infty$. The period is primarily sensitive to the dependence on the coupling latitude and the longitudinal location of the center of the wind stress anomaly pattern. There is also a dependence on the width of the wind stress with a local minimum (at about $\sigma = 20°$).

The resulting spatial patterns of the anomalies are displayed in Fig. 4, which shows a few snapshots of the anomalies in the North Pacific as an illustration of the typical time evolution. A large positive anomaly is stretching over the subtropics at year 100. The anomaly moves to the west and is replaced by an anomaly of opposite sign that arises in the east. All anomalies are bent to the west due to the faster Rossby wave speeds in lower latitudes. The anomalies in the subtropics are accompanied by weak anomalies of opposite sign to the north. In the observations the strength of the anomalies is reversed. Here, a strong anomaly in the midlatitude central Pacific is accompanied by weaker anomalies in the subtropics. The model behavior changes to a more realistic single maximum in the central North Pacific if we tune the model to a longer period by moving the coupling point farther north. Figure 5 shows the typical evolution for a coupling point at 38°N. The fact that the anomaly is stronger in the south is readily explained by the space-independent solution (3) of (1), which gives the relation $p(t) \sim t/f$: The Coriolis parameter f is smaller in the south and the growth rate is larger. In nature this effect may be masked by the much stronger wind stress curl anomalies in the north (see next section).

4. Model tuning

We will now try to tune our model closer to reality. The structure of the oceanic anomalies depends on the wind stress pattern. A more realistic pattern may be derived from observations or by GCM simulations. Here we use a structure that was obtained from an atmospheric GCM. LB94 performed a sensitivity study of the atmosphere to sea surface temperature anomalies (SSTA) using the ECHAM3 GCM (Roeckner et al. 1992). They found high sensitivity of this GCM to SSTA introduced in the central North Pacific. The wind response pattern of this model to such an SSTA in a perpetual January mode is shown in Fig. 6. The pattern resembles the wind stress anomalies related to the Pacific–North American pattern (PNA). In the following we use this wind stress curl pattern as the forcing structure X_0. It is much more difficult to find a reasonable relation between the thermocline depth anomaly p and the amplitude A of the wind stress. The experiment by LB94 gives a link between the SSTA in the central North Pacific and the wind anomalies. To incorporate this link in our model we have to specify a relation between the SSTA and the model's baroclinic pressure anomalies.

To find such a connection we force the ocean GCM HOPE (Latif et al. 1994) with observed wind stress and heat flux as derived by da Silva et al. (1994) from the Comprehensive Ocean–Atmosphere Data Set for the years 1949–94. The model SST was relaxed to the observed SST so that the model SST is always close to

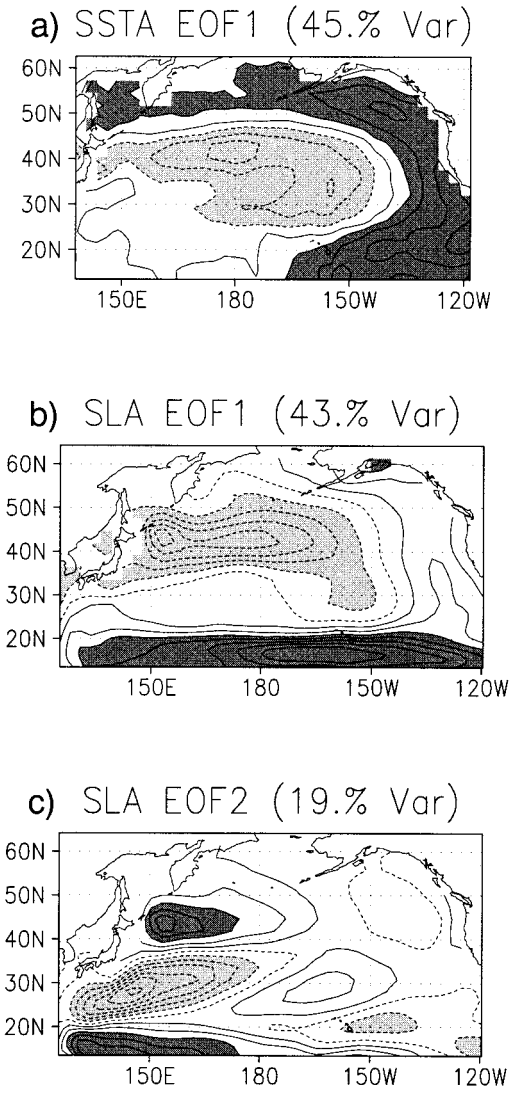

FIG. 7. (a) EOF of the observed SSTA. (b) First and (c) second EOFs of SLA, the ocean GCM HOPE forced with observed heat and wind stress anomalies. All data are filtered with a 5-yr running mean filter.

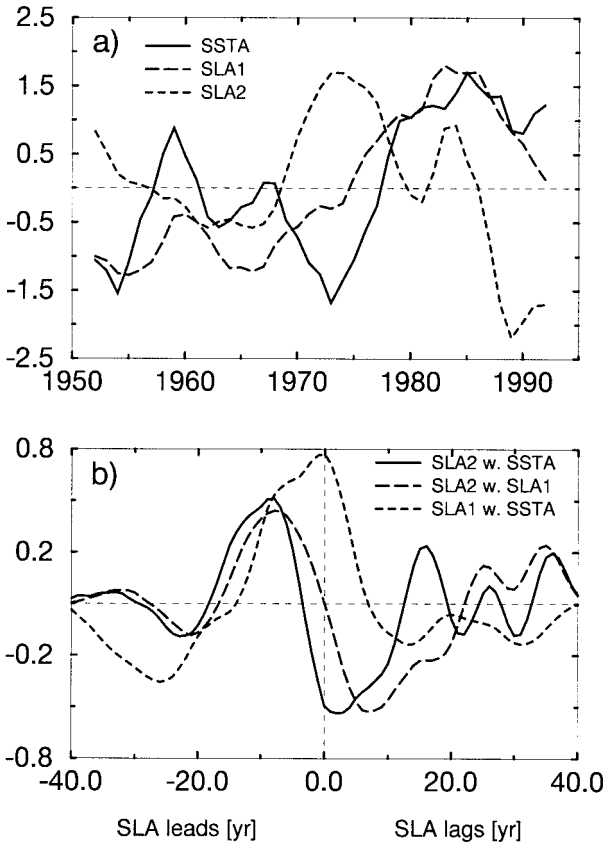

FIG. 8. (a) Principal component (PC) time series of the EOFs shown in Fig. 7. Solid: PC of first EOF of SSTA; long dashes: PC of first EOF of SLA; short dashes: PC of second EOF of SLA. (b) Lag correlation function of the PCs shown in (a). Solid: correlation of the PC 2 of SLA with the PC of SSTA EOF 1; long dashes: PC 2 of SLA with PC 1 of SLA; short dashes: PC 1 of SLA with PC of SSTA.

the observations. Figure 7 shows the first empirical orthogonal function (EOF) of the SSTA and the first two EOFs of the sea level anomalies (SLA). The data were filtered in time using a 5-yr running mean prior to the analysis. Both first–order EOFs show a large-scale signal in the central North Pacific that extends west up to the Asian coast. These EOFs explain a major part of the variance (45% and 43%) and manifest the decadal variability in the North Pacific. The second EOF of SLA has the strongest signal in the western part of the North Pacific at 30°N. The time series of the principal components (PCs) of the EOFs displayed in Fig. 7 are given in Fig. 8a. A lag correlation diagram of these PCs is shown in Fig. 8b. The sensitivity study of LB94 (see above) suggests that the major wind anomalies vary in phase with the first SSTA EOF. The first SSTA and SLA PCs have their maximum correlation at lag 0, that is, the first EOFs vary in phase. So the major wind anomalies and the first EOF of SLA vary in phase as well and the first SLA EOF may be interpreted as the instantaneous oceanic response to the changed Ekman pumping. The correlation between the SLA PCs 1 and 2 is maximum with PC 2 leading by 8 yr. As the first PCs of SLA and SSTA are in phase the maximum correlation between SLA EOF 2 and SSTA EOF 1 occurs around the same lead time.

So, if we couple in the western Pacific around the maximum of EOF 2, as above, these results suggest we should introduce an additional lag of around 8 yr between the sea level anomaly in this region and the wind stress amplitude *A*. This lag is consistent with the findings of Zhang and Levitus (1997). They investigated observed subsurface temperature measurements and found a lag of 5–7 yr between the first EOF of upper ocean temperature and the second EOF. Their second

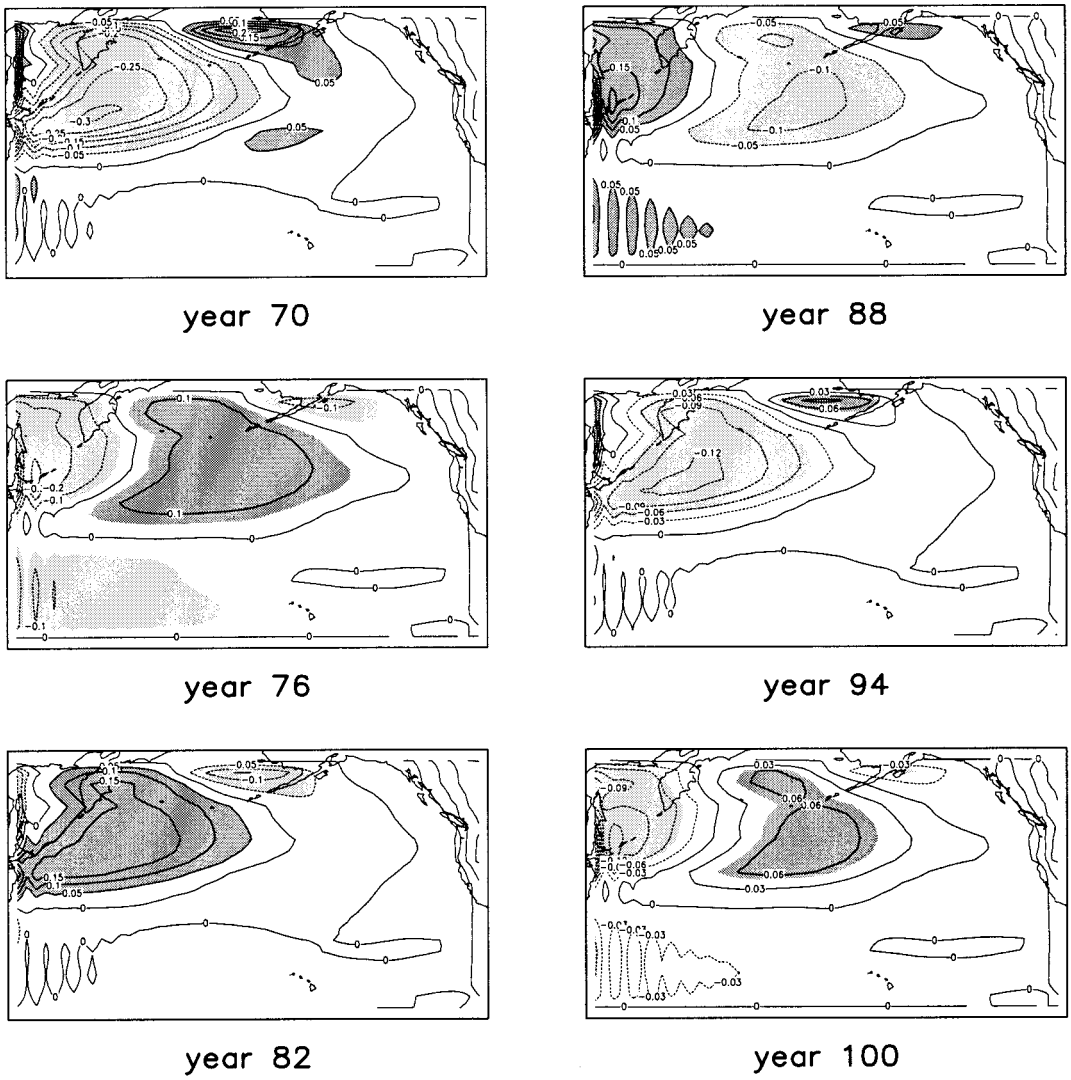

FIG. 9. Snapshots of thermocline depth anomalies using the wind stress pattern shown in Fig. 6 and a delayed feedback as defined in (9).

EOF has a maximum in the same area as EOF 2 of Fig. 7. So we use a delayed response of the atmosphere

$$A(t) = \alpha\overline{p}(\theta_1, \theta_2, \phi_1, \phi_2, t - t_d), \qquad (9)$$

where $\overline{p}(\theta_1, \theta_2, \phi_1, \phi_2, t)$ is the pressure anomaly of our model averaged over the region $\theta_1 < \theta < \theta_2$, $\phi_1 < \phi < \phi_2$ at time t. Figure 9 shows a few snapshots of the resulting sea level anomalies for $\theta_1 = 23°$N, $\theta_2 = 33°$N, $\phi_1 = 142°$E, $\phi_2 = 152°$E, $t_d = 8$ yr, and $\alpha = 1$. The anomaly patterns now look reasonable. A large positive anomaly is seen at year 76. it moves slowly to the west and is replaced by an emerging negative anomaly 12 yr later, which is again moving to the west. The location of the maximum of the anomalies is correct. However, the observed SSTA and subsurface anomalies stretch all the way to Japan (see Fig. 7a and Zhang et al. 1997) and are more or less stationary.

The period of the oscillations is approximately 25 yr. For $t_d = 0$ we found that the model oscillates with a period of 9 yr. The time lag we introduced prolongs the period of the model oscillations. A rough estimate of the model's period T is $T = 2(t_d + t_r)$ where t_r is the time the longest Rossby wave needs to reach the coupling area from the area of the excitation. This formula is easy to understand: Assume $t_d = 0$. An anomaly excited by the wind produces an anomaly of opposite sign after a time t_r when it reaches the coupling region. This new anomaly needs again a time t_r to reach the coupling area and to complete the cycle, which gives $T = 2t_r$. The introduction of the delay t_d increases the time until

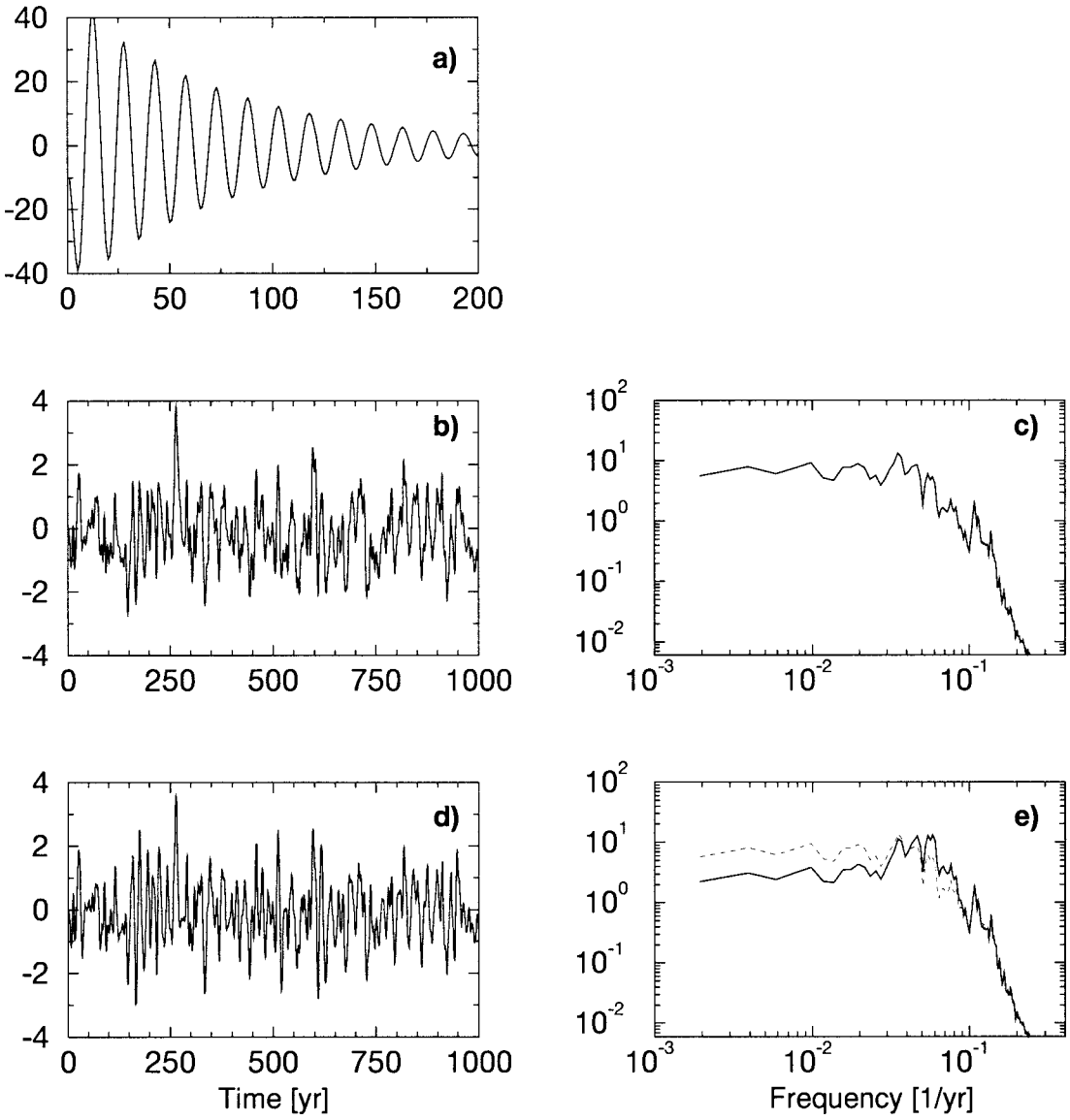

FIG. 10. Scaled time series and spectra of mean pressure anomalies in the index region 37°–39°N, 142°–150°E. The forcing used for (a) is the feedback of (8) with $\alpha = 0.2$. In (b) the forcing is white in time; $A(t)$ is white noise. (c) Shows the spectrum of (b). In (d) the forcings of (a) and (b) are superimposed. The spectrum of (d) is shown in (e) (solid). Spectrum (c) is redrawn in (e) (dashed) to ease comparison of the spectra.

an opposite signal is excited to $t_d + t_r$ so $T = 2(t_d + t_r)$ for a delayed wind response.

5. Stochastic forcing

Atmospheric weather noise is an important forcing component for the ocean. Frankignoul et al. (1997) show that stochastic forcing and Rossby wave dynamics can lead to a red spectrum of oceanic fields up to decadal timescales. Distinct spectral peaks, however, cannot be explained with such a simple model.

We incorporate stochastic forcing by the atmosphere in our model using a spatially coherent wind stress $F_s = W(t)X_0(\theta, \phi)$ which is uncorrelated in time, where $W(t)$ is white noise. The spatial pattern X_0 is the same as that used in the first experiment (Fig. 2). The resulting time series of p averaged over the index region 37°–39°N, 142°–150°E is shown in Fig. 10b. The time series is normalized to have unit variance. The spectrum of this time series is red (Fig. 10) as predicted by Frankignoul et al. (1997), and no decadal peak is visible.

This changes if we reintroduce the feedback discussed above. Again we use the feedback form of (9) with zero time lag ($\theta_1 = 35°$N, $\theta_2 = 37°$N, $\phi_1 = 142°$E, $\phi_1 = 152°$E, and $\alpha = 0.25$). The time series obtained in this case with feedback only is shown in Fig. 10a. We see

a weakly damped oscillation with a period of about 16 yr. As this is a transient behavior no spectrum is shown. We now add the stochastic forcing to this feedback system by using

$$A(t) = \alpha\overline{p}(t) + \gamma W(t),$$

with $\alpha = 0.25$ and $\gamma = 0.5$

The resulting normalized time series is shown in Fig. 10d and its spectrum in Fig. 10e. A broad spectral peak centered at a frequency of 0.06 yr^{-1}, that is, at a period of 17 yr is superimposed on the red spectrum of Fig. 10c. This is the scenario we like to propose for the decadal variability in the North Pacific and North Atlantic Oceans: a weakly damped coupled mode is excited by the stochastic forcing of the atmosphere.

6. Conclusions

We introduced a simple coupled model for the North Pacific. The ocean dynamics are based on the linear shallow water equations for the first baroclinic mode. The atmosphere forces the ocean by a fixed spatial wind anomaly pattern whose amplitude depends on the thermocline depth in the western part of the ocean basin.

With this kind of feedback the model shows oscillations on decadal timescales. In view of the model's simplicity the periods and structures of the anomalies agree reasonably well with observations. The introduction of random forcing by atmospheric weather leads to a red spectral response as predicted by Frankignoul et al. (1997). If feedback and noise are applied simultaneously to the ocean, a decadal peak is superimposed on a red spectrum as in the observed spectra.

Such a simple model lacks many aspects of the real world. Neither mean advection nor the boundary currents or atmospheric heat flux are included in our model. The lack of heat flux forcing and mean advection explains the reason why our anomaly moves westward, while observations and our GCM integrations show a more or less stationary SSTA pattern (Trenberth and Hurrel, 1994). Using an oceanic GCM coupled to a statistical atmosphere, Xu and Barnett (1998) showed that the heat flux contribution is significant in the development of the decadal fluctuations in the western Pacific. They also showed, however, that the heat flux is unnecessary for the development of decadal fluctuations. The heat flux influences the structure of the observed anomalies but is of minor dynamical importance. We also neglect the fast barotropic readjustment of the system. Liu (1993) showed that in his model this is the dominant effect in the northern regions where the thermocline is shallow.

A crucial aspect of our model is the way we couple the atmosphere to the oceanic thermocline depth anomaly. We use a simple point coupling or an area-averaged value of the thermocline depth in the western Pacific. This is a very crude way to model the feedback. However, this region is an area of strong surface temperature gradients causing cyclogenesis in the atmosphere (Roebber 1984). So it is plausible that the atmosphere is sensitive to temperature changes here. If the thermocline anomalies lead to an immediate SST change our model approach seems justified. However, our forced ocean GCM results presented in section 4 and observations (Zhang and Levitus 1997) suggest a lag of several years between the thermocline depth anomaly in the Kuroshio region and the SSTA and anomalous wind response. The inclusion of this lag prolonged the model's oscillation period. The question of how and where the atmosphere is most sensitive to midlatitude SSTA is far from being solved and deserves further research.

Acknowledgments. We thank two anonymous reviewers for helpful comments. This work was sponsored by NOAA via the Lamont/SIO Consortium program and the German Government under Grant 07VK01/1.

REFERENCES

Anderson, D. L. T., and A. E. Gill, 1975: Spin-up of a stratified ocean, with application to upwelling. *Deep-Sea Res.*, **22,** 583–596.

Bjerknes, J., 1964: Atlantic air–sea interaction. *Advances in Geophysics*, Vol. 10, Academic Press, 1–82.

da Silva, A., C. C. Young, and S. Levitus, 1994: *Atlas of Surface Marine Data 1994.* Vol. 1. National Oceanic and Atmospheric Administration, 83 pp.

Deser, C., M. A. Alexander, and M. S. Timlin, 1996: Upper ocean thermal variation in the North Pacific during 1970–1991. *J. Climate*, **9,** 1840–1855.

Douglas, A. V., D. R. Cayan, and J. Namias, 1982: Large-scale changes in North Pacific and North American weather patterns in recent decades. *Mon. Wea. Rev.*, **110,** 1851–1862.

Frankignoul, C., E. Zorita, and P. Müller, 1997: A simple model of the decadal response of the ocean to stochastic wind forcing. *J. Phys. Oceanogr.*, **27,** 1533–1546.

Gill, A. E., 1982: *Atmosphere–Ocean Dynamics.* Academic Press, 662 pp.

Graham, N. E., 1994: Decadal-scale climate variability in the tropical and North Pacific during the 1970s and 1980s: Observations and model results. *Climate Dyn.*, **10,** 135–162.

Hasselmann, K., 1976: Stochastic climate models. Part I. Theory. *Tellus*, **28,** 473–484.

Latif, M., and T. P. Barnett, 1994: Causes of decadal climate variability over the North Pacific and North America. *Science*, **266,** 634–637.

——, and ——, 1996: Decadal climate variability over the North Pacific and North America: Dynamics and predictability. *J. Climate*, **9,** 2407–2423.

——, T. Stockdale, J. O. Wolff, G. Burgers, E. Maier-Reimer, M. M. Junge, K. Arpe, and L. Bengtsson, 1994: Climatology and variability in the ECHO coupled GCM. *Tellus*, **46A,** 351–366.

Liu, Z., 1993: Thermocline forced by varying Ekman pumping. Part I: Spinup and spindown. *J. Phys. Oceanogr.*, **23,** 2505–2522.

Namias, J., 1959: Recent seasonal interactions between North Pacific waters and the overlying atmospheric circulation. *J. Geophys. Res.*, **64,** 631–646.

——, 1969: Seasonal interactions between North Pacific and the atmosphere during the 1960s. *Mon. Wea. Rev.*, **97,** 173–192.

Neelin, J. D., and W. Weng, 1998: Analytical prototypes for ocean–atmosphere interaction at midlatitudes. Part I: Coupled feedbacks as a sea surface temperature dependent stochastic process. *J. Climate*, in press.

Rhines, P. B., 1986: Vorticity dynamics of the ocean general circulation. *Annu. Rev. Fluid Mech.*, **18,** 433–497.

Roebber, P., 1984: Statistical analysis und updated climatology of explosive cyclones. *Mon. Wea. Rev.,* **112,** 1577–1589.

Roeckner, E., and Coauthors, 1992: Simulation of the present day climate with the ECHAM model: Impact of model physics and resolution. Rep. 93, 172 pp. [Available from Max-Planck-Institut für Meteorologie, Bundesstr. 55, 20146 Hamburg, Germany.]

Trenberth, K. E., 1990: Recent observed interdecadal atmosphere–ocean variations in the Pacific. *Bull. Amer. Meteor. Soc.,* **71,** 988–993.

——, and J. W. Hurrel, 1994: Decadal atmosphere–ocean variation in the Pacific. *Climate Dyn.,* **9,** 303–319.

Wallace, J. M., Y. Zhang, and K. Lau, 1993: Structures and seasonalitiy of interannual and interdecadal variability of the geopotential height and temperature fields in the Northern Hemisphere troposphere. *J. Climate,* **6,** 2063–2082.

Xu, W., and T. P. Barnett, 1998: Decadal variability in the North Pacific as simulated by a hybrid coupled model. *J. Climate,* **11,** 297–312.

Zhang, R. H., and S. Levitus, 1997: Structure and cycle of decadal variability of upper ocean temperature in the North Pacific. *J. Climate,* **10,** 710–727.